

Monitoring of rail short pitch corrugation using the time-frequency features of both vertical and longitudinal axle box accelerations

Li, Shaoguang; Zhang, Pan; Núñez, Alfredo; Dollevoet, Rolf; Li, Zili

DOI

[10.1016/j.measurement.2025.118064](https://doi.org/10.1016/j.measurement.2025.118064)

Publication date

2025

Document Version

Final published version

Published in

Measurement: Journal of the International Measurement Confederation

Citation (APA)

Li, S., Zhang, P., Núñez, A., Dollevoet, R., & Li, Z. (2025). Monitoring of rail short pitch corrugation using the time-frequency features of both vertical and longitudinal axle box accelerations. *Measurement: Journal of the International Measurement Confederation*, 255, Article 118064.
<https://doi.org/10.1016/j.measurement.2025.118064>

Important note

To cite this publication, please use the final published version (if applicable).
Please check the document version above.

Copyright

Other than for strictly personal use, it is not permitted to download, forward or distribute the text or part of it, without the consent of the author(s) and/or copyright holder(s), unless the work is under an open content license such as Creative Commons.

Takedown policy

Please contact us and provide details if you believe this document breaches copyrights.
We will remove access to the work immediately and investigate your claim.

Green Open Access added to TU Delft Institutional Repository

'You share, we take care!' - Taverne project

<https://www.openaccess.nl>

Otherwise as indicated in the copyright section: the publisher is the copyright holder of this work and the author uses the Dutch legislation to make this work public.



Monitoring of rail short pitch corrugation using the time-frequency features of both vertical and longitudinal axle box accelerations

Shaoguang Li, Pan Zhang, Alfredo Núñez, Rolf Dollevoet, Zili Li *

Section of Railway Engineering, Faculty of Civil Engineering and Geosciences, Delft University of Technology, Stevinweg 1, 2628 CN Delft, the Netherlands

ARTICLE INFO

Keywords:

Short pitch corrugation
Axle box acceleration
Wavelet spectrum
Maintenance support
Rail monitoring

ABSTRACT

This paper presents a methodology for detecting and monitoring short pitch corrugation (SPC) under varying measurement conditions using vertical and longitudinal axle box acceleration (ABA) measurements. The main objective of the detection algorithm is to determine the likelihood and approximate severity of SPC presence, providing insights for maintenance planning. The methodology combines a validated three-dimensional finite element (3D-FE) model of the ABA responses at SPC and signal processing techniques to extract meaningful data from the real-world on-board measurements. First, a 3D-FE vehicle-track model is validated and used to quantify the physical relationships in the time–frequency responses of ABA at SPC under different levels of corrugation severity and measurement speeds. Then, a measurement train is instrumented with multiple accelerometers to capture field data on ABA at SPC, which is validated with field inspections and Railprof measurements. Finally, the ABA responses are analyzed based on the number of signals detecting SPC and an assessment of severity based on impact energy due to SPC. The methodology is demonstrated by analyzing the track between Assen and Groningen on the Dutch rail network. Results show that the methodology accurately detects registered SPC locations. Further, a whole track analysis is conducted, from which the methodology proposes new locations and severities of SPC, providing crucial information for rail maintenance planning.

1. Introduction

Short pitch corrugation (SPC) is a type of rail periodic defect, commonly appearing on straight tracks or at gentle curves [1]. Its typical wavelength range is 20–80 mm, and amplitudes are in the order of dozens of micrometers. The presence of SPC increases vehicle-track system vibrations and contact forces between wheel and rail and results in faster degradation of the rail and railway track system components, e.g., fracture of fastening clips [2]. The emission of “roaring” noise by SPC brings much annoyance to residents living near railway tracks. Besides, SPC may induce the development of other rolling contact fatigue (RCF) problems like squats [3]. Because of its negative impacts on rail conditions, much research has been conducted to explain its mechanism for over a century. Still, the root causes of SPC are not yet completely understood due to its complexity [4]. For instance, field data show that SPC wavelength varies little with the train speed. However, when looking at different track locations with similar characteristics, SPC seems to have more preference for appearing in some places than in others. Li et al. [5] found that SPC initiation is attributed to longitudinal

compression modes of the rail. These vibrations, triggered by initial excitations such as the fastening system, consistently lead to the development of corrugation, providing an explanation for field observations in the Netherlands. This finding offers valuable insight for identifying effective solutions to prevent or mitigate SPC by strengthening rail longitudinal constraints [6]. At present, the most practically used countermeasure against SPC is grinding [7–9]. Grinding cannot be too often applied because it increases maintenance costs and reduces the life cycle of the rail. However, when grinding is applied too late, i.e., when severe SPC has developed, higher wheel-rail impact vibrations will happen, leading to faster development of rail defects that eventually will lead to rail replacements, or when it does not remove all residual material layer damage, there is a high chance that SPC will form again. Therefore, from both operational and economic considerations, it is necessary to develop an efficient monitoring method for SPC, especially a method that can detect SPC at an early stage, which can be used to plan the grinding maintenance and give an evaluation afterward. Grinding operations based on actual rail conditions can focus on locations where grinding is more needed and where it is most likely to be an effective

* Corresponding author.

E-mail address: z.li@tudelft.nl (Z. Li).

countermeasure.

There are different approaches to detecting rail defects. Generally, they can be categorized into human visual inspection, portable lightweight instrument measurement, and on-board measurement systems (conducted under loaded conditions) [10,11]. Traditional human visual inspection involves individuals walking along the track and visually identifying defects. This method is prone to human errors, impacts the safety of both inspector and railway operations, and is restricted by weather conditions [12]. Portable measurement equipment, which also requires a high level of human intervention on the railway track, can be further divided into two methods. One method involves collecting data from moving displacement transducers along a straight beam [13]. The other is a hand-pushed trolley that measures accelerations and evaluates the rail roughness with a double integration method [10]. An advantage of such measurement equipment is its high accuracy. For example, with corrugation analysis trolley (CAT), it is possible to measure corrugated rail with an accuracy higher than tens of micrometers [14]. The equipment can also measure acoustic roughness and evaluate rail conditions before and after grinding. However, in comparison to track recording vehicles, they are not efficient enough for continuously measuring large-scale railway infrastructures. Additionally, trolley-based systems cannot evaluate the wheel-rail dynamic interactions under a loaded condition, which provides a more precise qualification and quantification of the effective impact of rail defects on the railway system.

The train-borne inspection refers to the measurement system instrumented on running trains, such as axle box acceleration (ABA) [15,16], chord-based system [17,18], contact force measurement system [19], and video measurement systems [11,20,21]. The chord-based measurement system has been widely used for detecting rail irregularities as it is speed-independent, and there is no limitation on the minimum speed [11]. However, the system cannot represent the SPC well at certain wavelengths where the amplitude transfer function has a minimum of zero [11,18]. Therefore, it is necessary to evaluate the characteristics of the SPC in advance to choose the right parameters for the system. Secondly, due to the behavior of train lateral movement, the chord system may not always capture the same position on the railhead, which may influence the system performance regarding repeatability and reproducibility [17]. To address this problem, Chen et al. [17] introduced an automatic system to monitor and correct the position of the chord-based system, and the method shows high accuracy and robustness at a speed of 6 km/h. However, validation of results at higher measurement speed remains an open topic. Thirdly, the system performance can be influenced by the rainy weather, with water blocking the laser-camera window and water on the rail surface.

Video or the automatic visual inspection measurement system are based on high-resolution cameras capable of capturing the track images for defect identification [20,21]. In [11,21], the authors developed visual inspection systems to detect discrete rail defects. However, from images, it is not possible to quantify the depth of rail defects and estimate dynamic wheel-rail interactions, especially when defects are not visible. Furthermore, factors such as camera resolution, shutter speed, lighting, and track cleanliness may influence the detection results. In this paper, we are users of the ABA measurement equipment, which can capture wheel-rail vibrations at SPC under loaded conditions.

In the literature, ABA-based measurement systems have been applied to monitor railway infrastructure [22–24]. When the instrumented train runs over a rail defect, the impact of the defect is captured by the axle box acceleration. The ABA measurement system has been used to identify various types of local rail defects, including rail squats [25], poor-quality welds [26], and wheel flats [27]. While the ABA measurement system has proven effective in detecting most types of local defects, detecting and monitoring SPC requires further investigation. SPC typically appears along continuous rail sections and can be challenging to differentiate from general rail roughness. Furthermore, without a comprehensive understanding of how the axle box responds to

SPC excitation, the time–frequency characteristics necessary for detecting SPC under various measurement conditions would be unknown.

In [28], continuous track monitoring, which was installed on a DB in-service train, has been used to measure track geometry. This system is based on the axle box acceleration system, and it can measure the longitudinal level track geometry till the lower wavelength range of D0, i.e., 1 m based on EN13848-1 2019 [29]. Irregularities of wavelength shorter than 1 m are usually treated as rail roughness or rail corrugation. Grassie [29] pointed out that the ABA measurement system is applicable for the statistical evaluation of corrugation while not ideal for quantitative measurement. Faccini et al. [30] and Bocciolone et al. [20] examined the feasibility of using the vertical ABA measurement system to detect rail corrugation formed in curves of a metro system based on root mean square (RMS) values of ABA. Different from CAT, with which the corrugation profile can be quantitatively recreated with double integration, the train-borne ABA includes not only the impact vibration from the SPC but also complex structural vibration. Therefore, the direct integration of the ABA signals does not result in the actual SPC. In this paper, the ABA system considers both vertical and longitudinal ABA measurements. The detection of SPC is aimed at straight tracks as well as gentle curves with insignificant speed variation and lateral interactions. In addition, a physical model is proposed to understand and validate the ABA measurement results, facilitating the detection and assessment of SPC.

Preliminary findings regarding the use of vertical ABA for detecting SPC were presented in [31]. In this paper, we expand the analysis to include both vertical and longitudinal ABA. Moreover, the 3D FE vehicle-track model is validated for both vertical and longitudinal ABA. Additionally, we conduct a sensitivity analysis of ABA at SPC under different train speeds, evaluate grinding operations, and present more extensive detection results. This paper is structured as follows. Section 2 introduces the ABA measurement system and instrumentation. Section 3 examines the time–frequency responses of SPC using a 3D FE vehicle-track model and identifies the time–frequency response of ABA at SPC. In Section 4, a detection methodology of SPC is proposed using multiple ABA measurements and the responses as obtained from the 3D-FE model. The monitoring of the corrugation is characterized by determining the presence of SPC and assessing its severity based on the ABA energy signal at the detected locations. Section 5 shows the results of the methodology applied to the Dutch railways between Assen and Groningen. Finally, some conclusive remarks and further research are presented.

2. ABA measurements for detection of SPC

SPC is identified as periodic bright peaks and dark valleys along the central running band of the rail surface. SPC is characterized by its wavelength and severity. Unlike isolated rail defects, SPC appears continuously along the track, resulting in impact vibrations over longer distances. Therefore, an effective SPC detection method should not only identify the locations where SPC starts and ends but also assess its severity. To achieve this, a methodology that combines both ABA instrumentations together with knowledge about the responses of the physical system is necessary. In this section, the key aspects of ABA measurement systems are presented.

2.1. ABA measurement system

To facilitate comprehensive measurements, both vertical and longitudinal ABA accelerometers are installed on each wheelset (leading and trailing) of the bogie for both the left and right rails. The inclusion of longitudinal signals has been shown to improve the detection hit rate of light rail squats, as reported in [25]. Two accelerometers on each axle box are differentiated based on their respective mounting angles: 90° – accelerometer in the vertical direction to the train running direction and

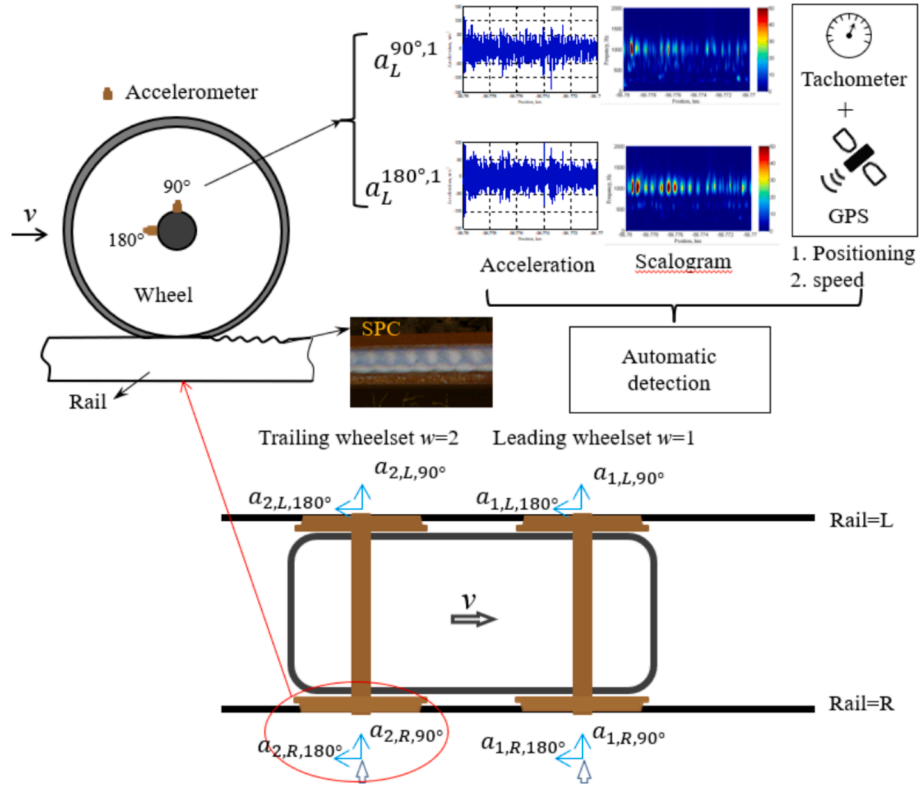


Fig. 1. Schematic diagram of the instrumentation of accelerometers and detection procedure.

Table 1
Accelerometers with consideration of the wheelset and accelerometer angles.

Wheelset	Angle of accelerometers	
	90°	180°
Leading wheelset ($w = 1$) left side	$a_{1,L,90^\circ}$	$a_{1,L,180^\circ}$
Trailing wheelset ($w = 2$) left side	$a_{2,L,90^\circ}$	$a_{2,L,180^\circ}$
Leading wheelset ($w = 1$) right side	$a_{1,R,90^\circ}$	$a_{1,R,180^\circ}$
Trailing wheelset ($w = 2$) right side	$a_{2,R,90^\circ}$	$a_{2,R,180^\circ}$

180° – rear accelerometer opposite to the train running direction. Each accelerometer is assigned a unique label that indicates the side of the rail it measures (left and right) and the mounting angle. Consequently, an acceleration signal is denoted as $a_{w,r,\theta}(t)$, where angle $\theta \in \{90^\circ, 180^\circ\}$, rail $r \in \{L, R\}$ indicating left (L) or right (R) rail, $w = 1, \dots, W$, indicating the wheel number, and t representing the time of measurement. Global positioning system (GPS) and tachometer readings are recorded to provide the information of the actual kilometer position in track $x(t)$ and the train's speed $v(t)$. As the wheelset is rolling over the rail surface with defects, vibrations resulting from the impact of rail defects are captured

by the acceleration sensors through the axle box. The clock of the ABA system is synchronized with the GPS clock. Then, rail defects can be located by matching ABA with locations in the track to facilitate track maintenance. During the measurements, the sampling frequency was 25.6 kHz and the train speed was approximately 100–110 km/h.

The instrumentation of the ABA measurement system and the corresponding detection procedure are shown in Fig. 1. To differentiate the accelerometers from different wheels and mounting angles, each accelerometer is given a name, as shown in Table 1.

2.2. Wavelet transform based time–frequency analysis

ABA signals from the wheel-rail interaction are non-stationary, especially with rail anomalies. To effectively identify and detect rail defects, it is essential to perform time–frequency analysis on these signals. In this paper, the continuous wavelet transform (CWT) is employed to analyze the time–frequency distribution of the ABA signals [32], as defined below [33],

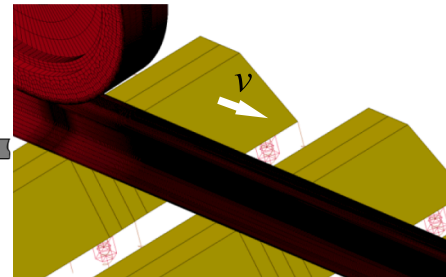
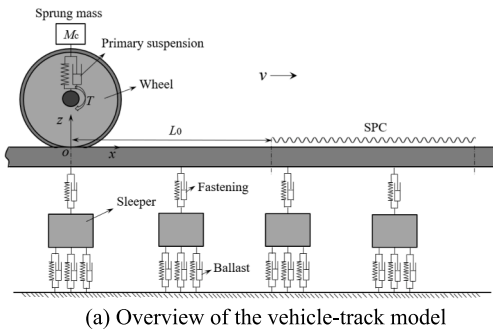


Fig. 2. 3D FE vehicle-track model.

Table 2
Vehicle parameters and track parameters.

Parameters	Values	Parameters	Values
Sprung mass	7200 kg	Wheel and rail material	Young's modulus 210 GPa
Primary suspension	Stiffness 1.15 MN/m	Sleeper	Poisson's ratio 0.3
	Damping 2.5 kNs/m		Density 7,800 kg/m ³
Railpad	Stiffness 1,300 MN/m	Young's modulus	38.4 GPa
	Damping 45 kNs/m		Poisson's ratio 0.2
Ballast	Stiffness 45 MN/m	Mass density	2520 kg/m ³
	Damping 32 kNs/m		Spacing (<i>L</i>) 0.6 m

$$CWT_{w,r,\theta}(s, \tau) = \frac{1}{\sqrt{s}} \int_{-\infty}^{\infty} a_{w,r,\theta}(t) \psi^* \left(\frac{t - \tau}{s} \right) dt \quad (1)$$

Where $CWT_{w,r,\theta}(s, \tau)$ are wavelet coefficients for the signal $a_{w,r,\theta}(t)$ to be analyzed, ψ^* is a family of wavelets from the mother wavelet $\psi(t)$ by a translation of τ and a wavelet scaling of s and $*$ indicates a complex

conjugate. The wavelet power spectrum (WPS), or scalogram, is defined as the square of wavelet coefficients, expressed by $|CWT_{w,r,\theta}^2(s, \tau)|$. It provides position, frequency, and wavelet energy information of a vibration signal.

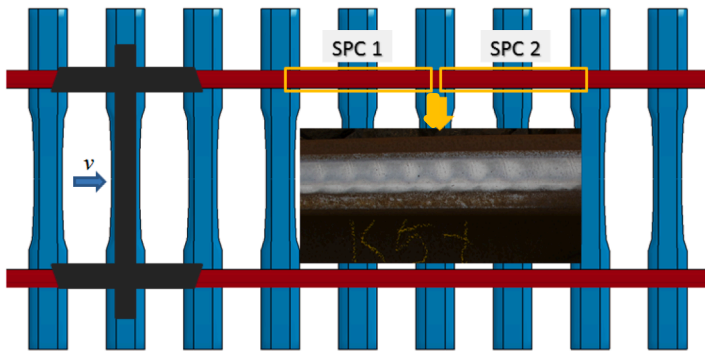
In the following section, an analysis is conducted with a 3D dynamic finite element (FE) vehicle-track model to establish a clearer connection between the scalogram and SPC, to gain a more accurate understanding of the frequency responses at various measurement speeds.

3. Physical responses of SPC using the FE model

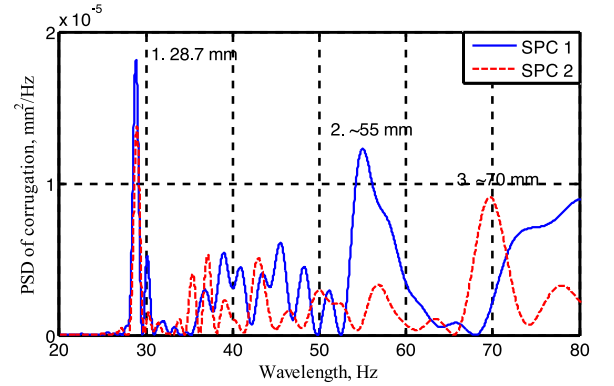
3.1. FE model

We consider a dynamic 3D FE vehicle-track model of the Dutch railway tracks. The model was built with the software Ansys/Ls-Dyna to study the transient vehicle-track interaction when the wheel rolls over a rail surface with SPC [34]. The frequency responses of the axle box acceleration signals obtained from this model will be validated, analyzed, and used as inputs for detecting SPC in this paper.

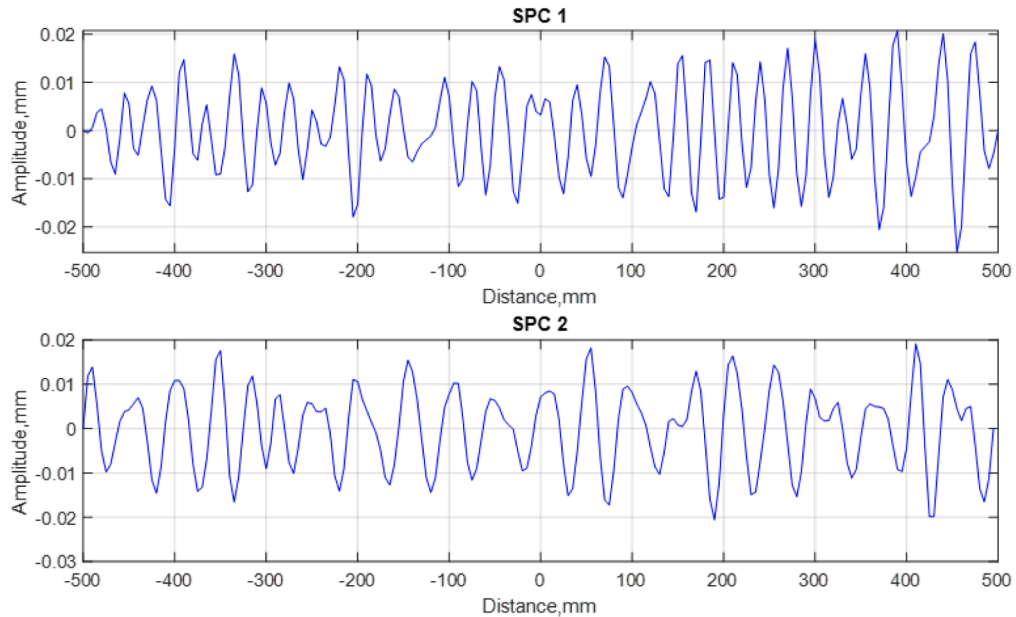
Fig. 2a presents a schematic diagram of the FE model. The vehicle structures above the primary suspension are simplified into mass elements. The primary suspension, the fastening system, and the ballast are represented by spring-damper elements. The wheel, rail, and sleepers



(a) SPC measurement locations and profiles



(b) PSD of the measured SPC profile



(c) Distribution of the measured SPC in spatial domain

Fig. 3. Schematic diagram of field measured SPC and their PSD distributions.

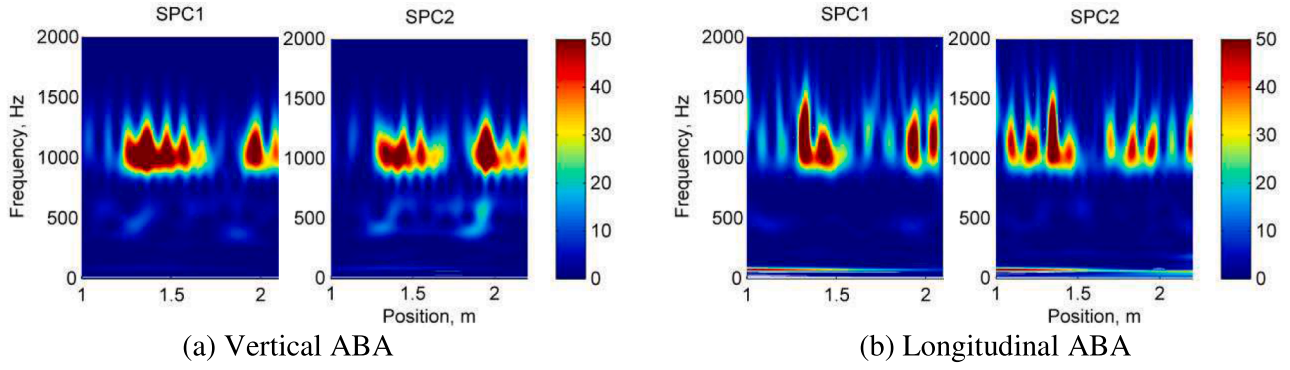


Fig. 4. Scalograms of the ABA signals from the FE model.

are modeled using 3D solid elements (see Fig. 2b). The radius of the wheel is 0.46 mm with a 1/40 conicity. The rail is UIC 54 with a 1/40 inclination. The sleeper spacing is 0.6 m, and the total track length is 20 m. The contact between the wheel and rail is treated as surface-to-surface contact utilizing a penalty contact algorithm. The model employs a friction coefficient of $f = 0.4$. Other system parameters are from the typical Dutch railway and are shown in Table 2. A traction coefficient μ of 0.1 is used in this paper. For comparison with the measured ABA, the acceleration signal is exacted at a node located on the axis of the wheel axle, which is proven to be accurate in [35]. A procedure combining implicit and explicit methods simulates the dynamic interaction between the vehicle and the track. A small time step of 7.09118×10^{-8} s is set to meet the Courant stability criterion [36]. To ensure that the initial oscillations caused by the imperfect static equilibrium are sufficiently damped and relaxed before the wheel enters the solution zone (SPC zone), an initial distance of $L_0 = 1$ m is introduced.

3.2. Measurement of rail SPC profile

To investigate the vibrations induced by SPC at the wheel-rail interface, actual rail SPC profiles were measured using RAILPROF

[13] and utilized as inputs in the FE model to analyze the dynamic responses of the vehicle-track system, specifically the ABA values obtained from numerical simulations. The RAILPROF equipment measures the longitudinal-vertical profile of the rail by employing a displacement transducer that moves along a 1 m straight frame positioned on the rail. In the case of UIC 54 rail, it measures the longitudinal-vertical rail profile at the center of the rail crown, as the SPC is mainly observed in the middle of the railhead.

Fig. 3a illustrates the locations of the SPC measurements with RAILPROF. The maximum peak to trough distance in the SPC profile is less than 100 μm . Further analysis, presented in Fig. 3b, demonstrates the power spectral density (PSD) of the SPC profiles, revealing three prominent wavelength components: approximately 28.7 mm, ~ 55 mm, and ~ 70 mm. Note that both SPC 1 and SPC 2 exhibit a predominant wavelength component at 28.7 mm, while SPC 1 displays a localized secondary component at around 70 mm. Over a longer distance, the 28.7 mm SPC wavelength corresponds to the corrugation observed in Fig. 3a and will be the focus of the analysis.

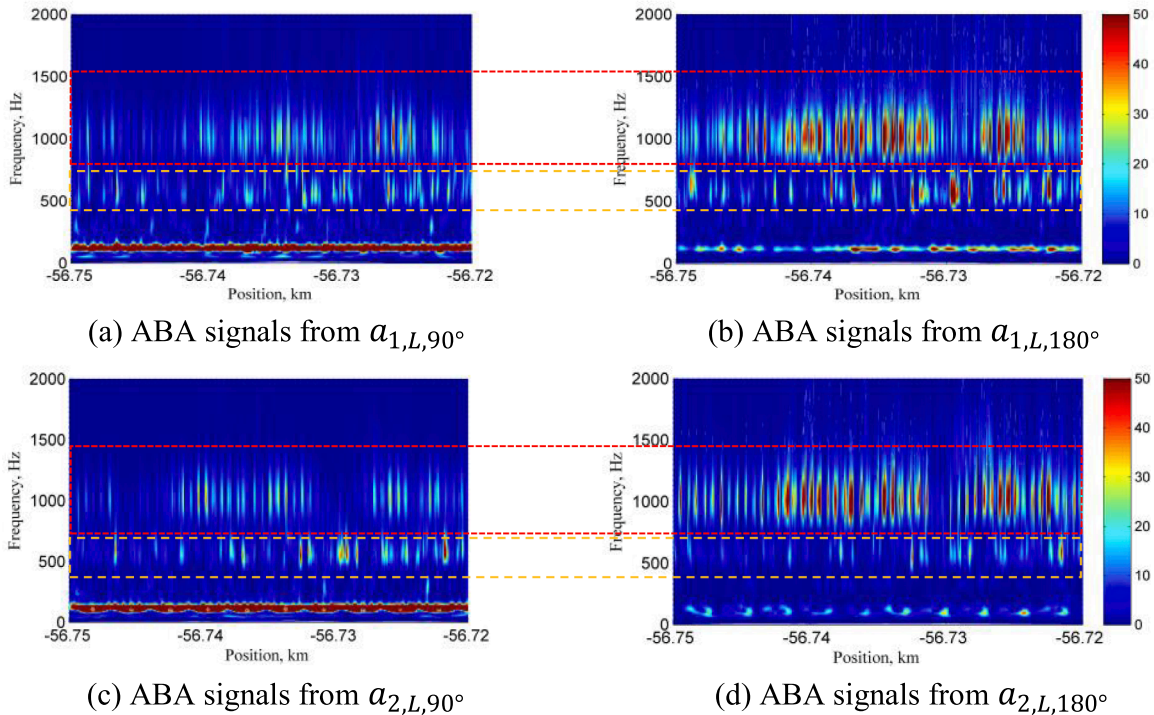


Fig. 5. Scalogram of ABA signals for accelerometer sensitivity analysis to the SPC ($v = 102.6$ km/h).

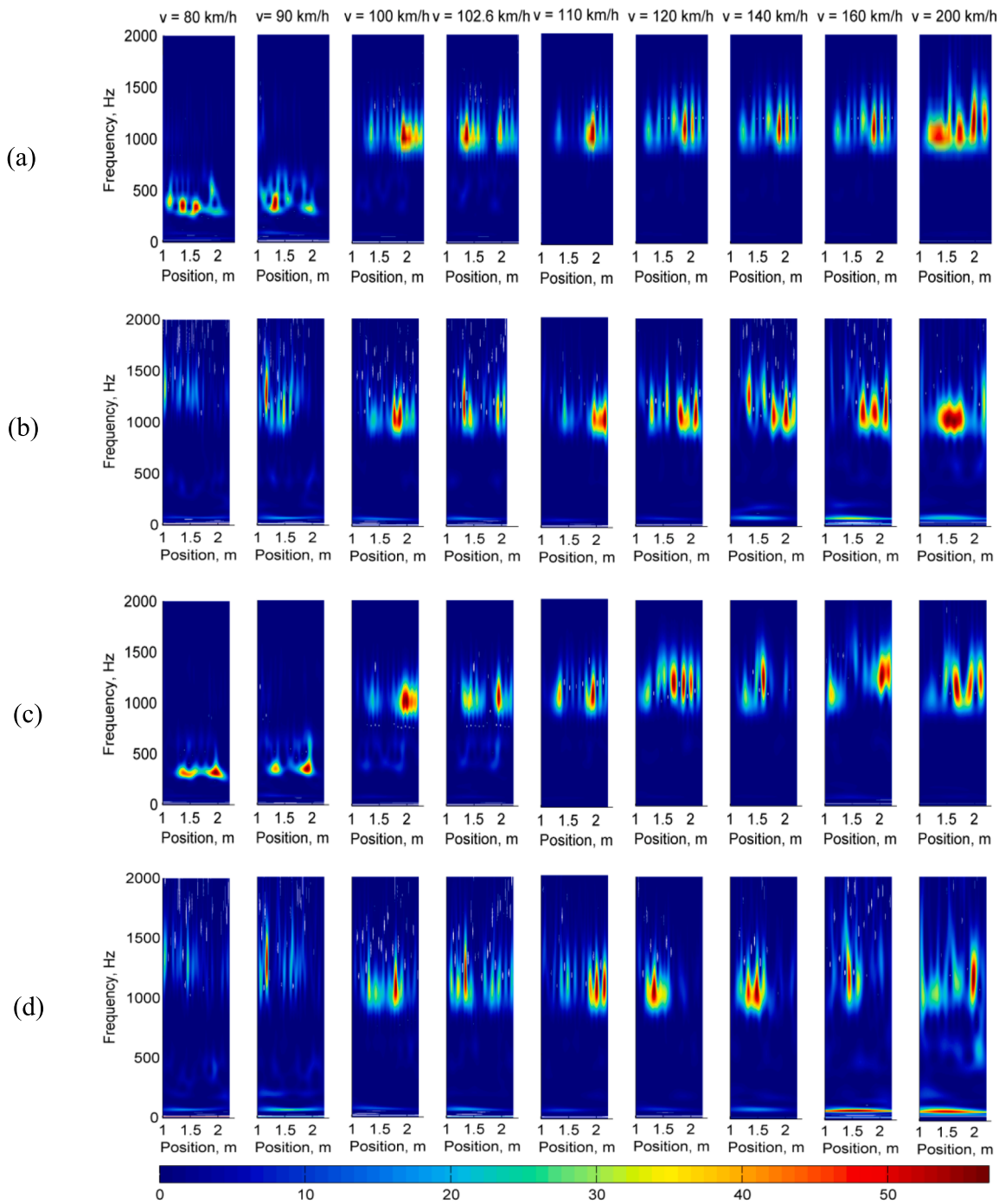


Fig. 6. Scalograms of the simulated ABA signals with (a) vertical ABA at SPC 1, (b) longitudinal ABA at SPC1, (c) vertical ABA at SPC 2, and (d) longitudinal ABA at SPC2 under the variation of vehicle speeds.

3.3. Numerical simulation of ABA at SPC and validation

Before the analysis below, it is important to note that the ABA signals simulated with the 3D-FE model capture both the forced vibrations from SPC (dependent on speed and corrugation wavelength) and structural resonances from the vehicle-track system (dependent on system modal properties). Compared to structural resonances, forced vibrations exhibit relatively lower energy concentration—particularly under very light corrugation conditions. Consequently, for corrugation detection, structural resonances serve as the primary indicator. In the frequency domain up to 2000 Hz, it is known from [5,36,37] that key resonances include:

- Full track or P2 resonance at ~ 90 Hz
- Sleeper anti-resonance at ~ 320 Hz
- Rail resonance at ~ 1000 Hz
- Pinned-pinned resonance at ~ 1180 Hz
- Longitudinal rail vibrations, e.g. 1360 Hz

The ABA signal is obtained through a transient simulation where a wheel rolls over a rail surface with SPC. The vehicle speed in the simulation is initially set to 102.6 km/h to match the measurement train. Fig. 4 shows the wavelet power spectrum (WPS) of the simulated ABA signals for both vertical and longitudinal directions at two different SPC inputs.

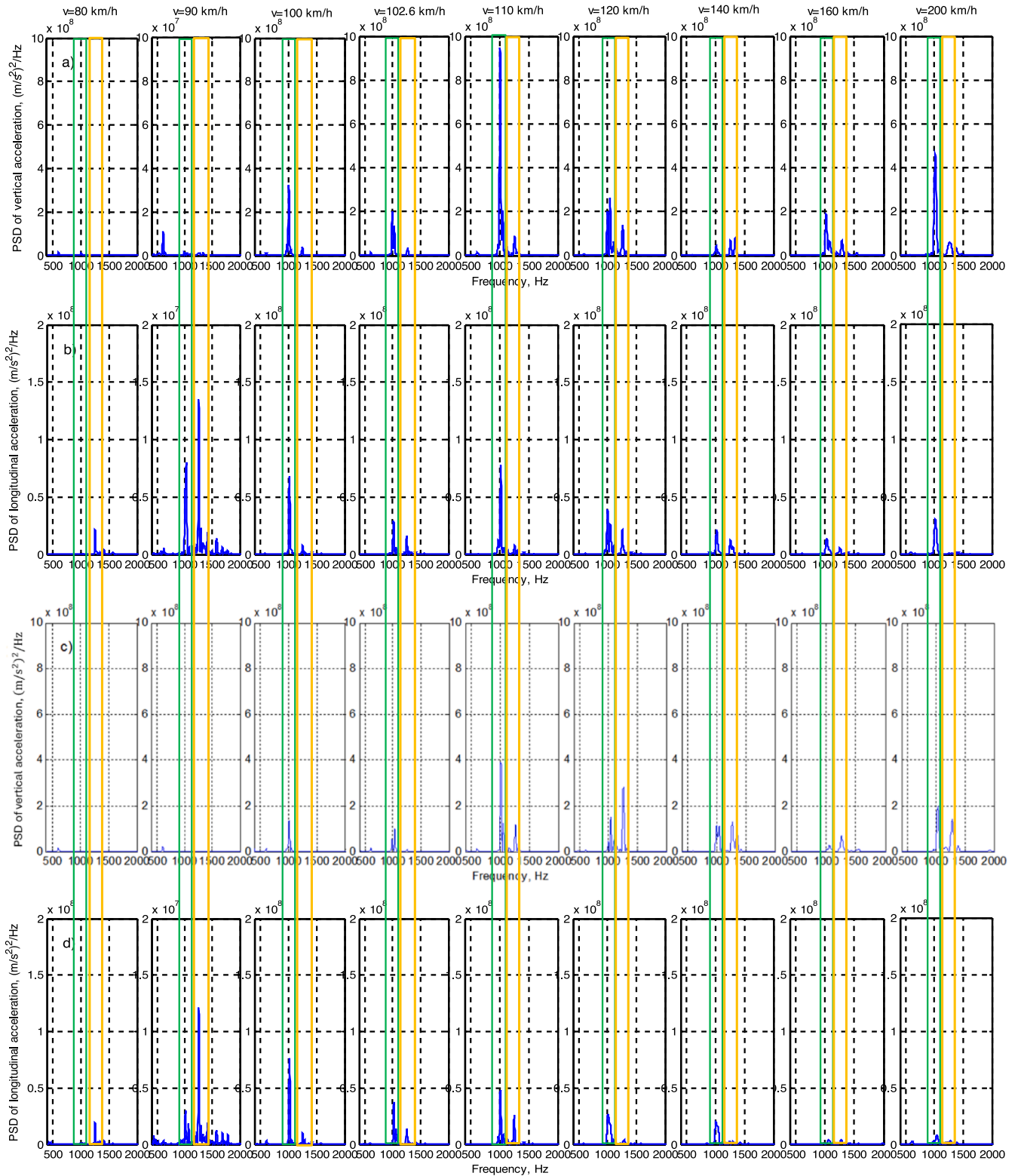


Fig. 7. PSD of simulated ABA with SPC 1 and 2 at different speeds, (a) vertical ABA at SPC 1, (b) longitudinal ABA at SPC1, (c) vertical ABA at SPC 2, and (d) longitudinal ABA at SPC2 under the variation of vehicle speeds (green block highlights the frequency around 1000 Hz and the orange block highlights the frequency around 1250 Hz). (For interpretation of the references to colour in this figure legend, the reader is referred to the web version of this article.)

The results reveal a dominant vibration energy concentration at approximately 1000 Hz, corresponding to rail bending and pinned–pinned resonances, and a secondary component around 500 Hz, likely linked to force vibration excited by SPC with the 50 mm and 70 mm wavelength components. These components arise from the

interaction between SPC-induced excitation and modal properties of the track.

Fig. 5 presents the measured ABA signals with SPC at the same speed (102.6 km/h). Both vertical and longitudinal ABA exhibit dominant frequency ranges from 700–1600 Hz, which agrees well with simulation

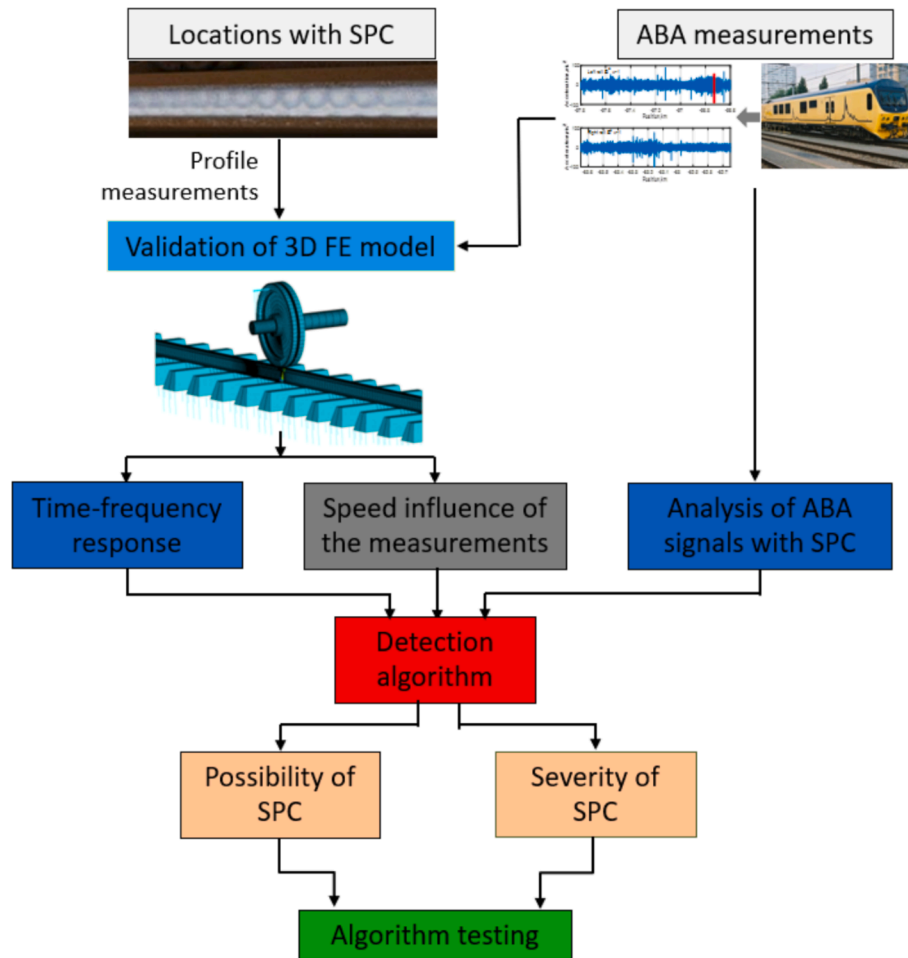


Fig. 8. Flowchart of the detection algorithm of SPC.

results. Notably, the longitudinal ABA demonstrates greater sensitivity to SPC in this frequency band, which aligns with the measurement results in [24] that longitudinal ABA is more sensitive in detecting light squats with shorter wavelengths of about 10–30 mm.

A secondary frequency component, less visible in simulations, is also observed in the measured data. Furthermore, a ~ 100 Hz component appears in vertical ABA, associated with P2 resonance. This component is excluded from the detection algorithm as it lies outside the SPC frequency range of interest.

These results validate that the dominant wavelength range of 700–1600 Hz in both simulation and measurement is a reliable indicator of SPC, while also acknowledging the presence of structural vibration modes that may overlay or interact with SPC responses.

3.4. Influence of the speed variation

To investigate the influence of varying train speeds on the detection of SPC, the 3D FE vehicle-track model incorporates speed variations. Fig. 6 illustrates the results of simulations conducted on the ABA response at SPC 1 and SPC 2 under different speeds. In the vertical ABA, two main frequency bands are observed. At speeds of 80 km/h and 90 km/h, there is a comparatively lower frequency band at 200–400 Hz, which is attributed to the anti-sleeper resonance being excited by the longer corrugation wavelengths. At speeds ranging from 100 km/h to 200 km/h, another frequency band emerges around 700–1600 Hz. In the longitudinal ABA, however, the dominant frequency range for SPC is consistently around 700–1600 Hz across the entire speed variation range. From the figures, it can be concluded that when the measurement

train speed is below 90 km/h, the vertical ABA response at 1000 Hz is weaker than at lower frequencies, associated with the rail resonance and pinned–pinned resonance excited by the shorter corrugation wavelength (28.7 mm). In such cases, the main energy concentrates at about 400 Hz, where the useful information can be submerged by a high energy concentration at a low frequency at a lower speed. On the other hand, the longitudinal ABA signals can capture the frequency characteristic of SPC over a wider range of speeds.

To further emphasize the axle box acceleration (ABA) responses within the 700–1600 Hz range under varying speeds, Fig. 7 illustrates the PSD of simulated acceleration signals for speeds ranging from 80 km/h to 200 km/h. At speeds below 90 km/h, the vertical ABA response around 1000 Hz is minimal compared to that observed at higher speeds. This is likely due to insufficient excitation from rail corrugation at lower speeds, which fails to induce structural resonance near this frequency. As the speed increases to 100 km/h, spectral components near 1000 Hz begin to emerge, and at 110 km/h, the response reaches its maximal value. In contrast, the longitudinal ABA consistently exhibits notable responses across the 700–1600 Hz range, even at the lowest simulated speed of 80 km/h, indicating a high sensitivity to excitation that appears largely independent of train speed, meaning a more robust method for detection.

4. SPC detection with ABA signals

Based on the identified time–frequency characteristics under different speeds from the FE simulations, an SPC detection algorithm is formulated using the measured ABA signals, as shown in Fig. 8. The

detection algorithm enables the identification of SPC locations in terms of different possibilities: SPC, high possibility of SPC, low possibility of SPC, and no SPC. For those places with detected SPC, a severity value is proposed for the ABA energy signal. Two locations with SPC are used as examples to validate the algorithm. Finally, the validated algorithm is used to detect SPC in a longer track section up to 15 km where the measurement speed is roughly 100–110 km/h.

Specifically, the scale-averaged wavelet power (SAWP) is employed, as a method for detecting SPC. SAWP is defined as the calculated sum of the weighted wavelet power spectrum (WPS) within the frequency range of f_1 to f_2 [37].

$$SAWP_{w,r,\theta}(t) = \frac{\delta_j \delta_t}{C_\delta} \sum_{j=f_1}^{f_2} \frac{|CWT_{w,r,\theta}^2(s_j, t)|}{s_j} \quad (2)$$

where n is the time index, δ_j and δ_t are the scale step and time step respectively, and C_δ is an empirically derived constant for each wavelet function.

The SAWP is evaluated in the frequency range that is specifically targeted for SPC detection. It's important to note that the frequency range might be influenced to some extent by the track structure. Consequently, in a more comprehensive framework, the scales should vary per location $s_j(x(t))$. Furthermore, impact vibrations from other isolated defects, which exhibit responses similar to SPC frequencies, do not bear the continuous vibrational features in the signals. Furthermore, defects from the wheel can be identified easily and removed [25], and background noises do not have a strong influence on the frequency range of SPC. Therefore, SPC can be identified through a pre-analysis of the measured signals, and the automatic detection algorithm can be adjusted based on the frequency of SPC responses.

The spatial series of the SAWP with maximum values within a designated frequency range at certain locations exceeding a certain threshold are detected as isolated defects, such as squats [25]. In the case of SPC, it is more reasonable to detect it by providing an indication of a distance range. Let's define a function $H_r(x)$, with rail $r \in \{L, R\}$, that equals 1 if the rail at location x is affected by SPC, and 0 otherwise.

Four variables are introduced for the purpose of SPC detection:

1) As there is an overlap in the time–frequency responses of singular defects with SPC, to reduce false positive detections, the SAWP is evaluated around a finite distance (Δ_{SPC}) from the location $x(t)$,

$$[x(t) - 0.5\Delta_{SPC}, x(t) + 0.5\Delta_{SPC}]$$

2) A threshold $Th(v(t))$ that is train speed dependent is defined based on the averaged energy intensity of SAWP within the range Δ_{SPC} . If the sum of SAWP within Δ_{SPC} is above the threshold $Th(v(t))$, the accelerometer (defined by *angle*, *w*, *rail*) will trigger one detection of SPC at location $x(t)$.

$$H_{w,r,\theta}(t, x(t), v(t)) = \begin{cases} 1 & \text{if } \sum_{x(t)=x(t)-0.5\Delta_{SPC}}^{x(t)=x(t)+0.5\Delta_{SPC}} SAWP_{w,r,\theta}(t, x(t), v(t)) \geq Th(v(t)) \\ 0 & \text{Otherwise} \end{cases} \quad (3)$$

Note that the threshold is a relative, empirical, and data-driven parameter, rather than an absolute physical measure, and can be dynamically adjusted to modify the sensitivity of the algorithm. When considering all the accelerometers, the sum of the number of predictions as SPC is represented by N_{SPC} .

3) The number of predictions as SPC from different accelerometers and channels, wheels and test runs indicate the possibility of SPC occurrence in the track, $P_{SPC}(x(t))$. Depending on the ratio between N_{SPC} and the total number of measurement signals N_{total} , $P_{SPC}(x(t))$ is defined

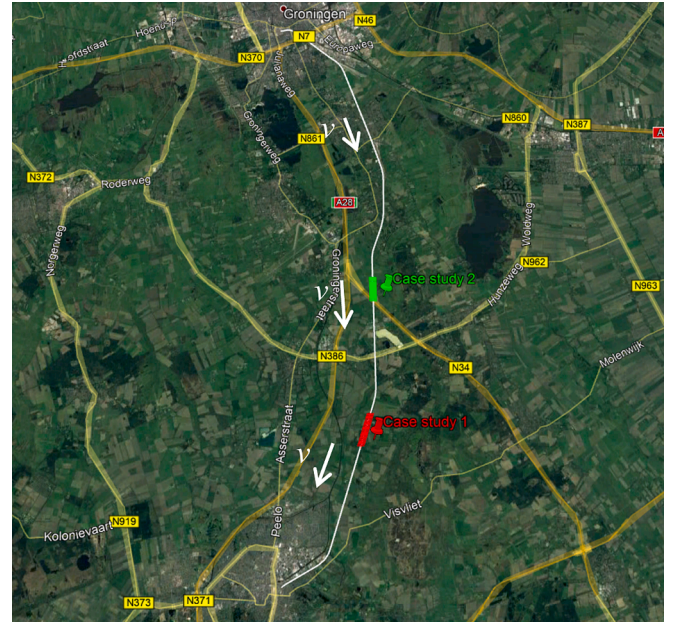



Fig. 9. Track between Assen-Groningen shown in Google map ‘’ (— Case Study 1, — Case Study 2).

with 4 levels: SPC, higher possibility SPC, lower possibility SPC and No SPC. The tuning parameters a and b such as $0 < b < a < 1$ represent the thresholds between the different qualitative levels.

$$P_{SPC}(x(t)) = \begin{cases} SPC & \text{if } N_{SPC} = N_{total} \\ High\ possibility\ SPC & \text{if } aN_{total} \leq N_{SPC} < N_{total} \\ Low\ possibility\ SPC & \text{if } bN_{total} \leq N_{SPC} < aN_{total} \\ No\ SPC & \text{if } N_{SPC} < bN_{total} \end{cases} \quad (4)$$

The classification criteria are heuristic and currently serve as a practical decision support tool.

4) In addition, the severity of the SPC is shown with the value of SAWP within the Δ_{SPC} . The definition regarding the corrugation severity from light, to moderate and severe is part of the further research.

These four parameters can be adjusted according to the actual conditions of ABA signals with SPC and maintenance needs. Further, the parameters for corrugation possibility and severity are used to showcase results. These parameters can be further customized to meet specific requirements. Within the given equations, speed is considered as a parameter in the detection algorithm for the overall algorithm. In the measurement campaign, the speed remained within the range where no adjustments to the speed were necessary.

5. Algorithm testing and validation

The frequency range corresponding to the SPC studied in this paper is 700–1600 Hz. To minimize the false positive prediction of rail squats as SPC, which can occur due to high energy concentration, SAWP is evaluated within a 10-meter distance. If the SAWP within the 10 m exceeds 1.25 times the average SAWP per 10 m calculated over the entire measurement section with approximately the same speed, denoted as

$$Th = 1.25 \left(\sum_{x(t)=x(t)-0.5\Delta_{SPC}}^{x(t)=x(t)+0.5\Delta_{SPC}} SAWP \right)_{avg}, \text{ the track location will be}$$



(a) SPC at the location of case study 1



(b) SPC at the location of Case Study 2

Fig. 10. SPC in Case Studies 1 and 2.

predicted as having SPC. The adopted threshold was determined through a trial-and-error process, and found to effectively distinguish SPC-affected areas from normal track segments, minimizing false positives in our specific cases. Additionally, two more thresholds are defined to assess the possibility of SPC. The total number of signals used for prediction is determined by multiplying the number of accelerometers by the number of measurements. If all signals indicate SPC, the prediction is considered certain. If more than 50 % of the total signals show a 10 m section as SPC, then it is categorized as having a higher possibility of SPC. If more than 33 % of the total signals indicate an SPC section, it is classified as having a lower likelihood of SPC. When the

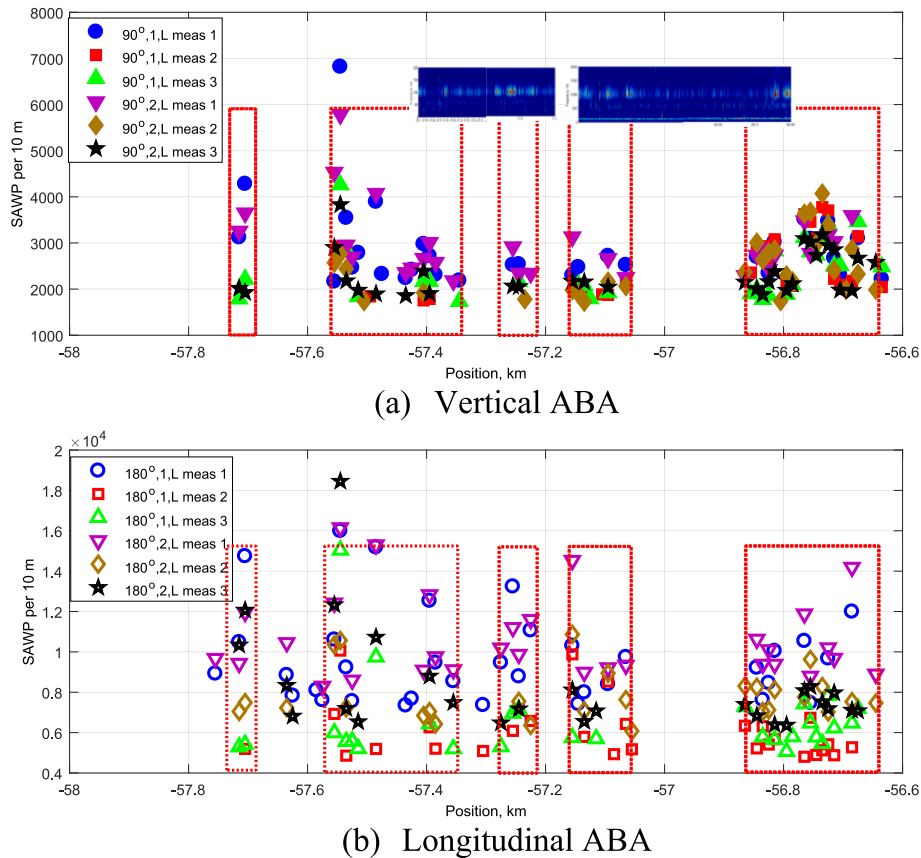
number of signals indicating SPC is less than 1/3 of the total signals, the section is defined as not having SPC. In addition to predicting the possibility of SPC, the severity of SPC is also represented by the SAWP per 10 m for those sections classified with a higher possibility of SPC. A threshold can be established to differentiate between SPCs of varying severities.

In order to test the algorithm, two specific locations on a track known to have SPC have been selected as case studies. The track is between Assen and Groningen in the Netherlands, as shown in Fig. 9 with a white line. On the map, these two locations are highlighted in different colors, with one marked in red and the other in green. Notably, both locations are situated on straight sections of the track. Fig. 10 provides a visual representation of the rail surface corrugation observed at these two locations.

5.1. Case Study 1

Fig. 5 displays the time–frequency response of the ABA measurements, with the key frequency components associated with SPC. By utilizing the acceleration signals as input for the detection algorithm, the prediction of SPC is obtained, as illustrated in Fig. 11 with the channels of signals predicted as SPC and with their respective SAWP per 10 m. Please note that due to the presence of corrugation only on the left rail, the analysis of the right-side rail is not shown in the results.

Fig. 12a and b show the prediction of SPC in terms of possibility and SAWP per 10 m to reveal the severity, respectively. To assess the possibility of SPC in the prediction, two thresholds are applied, with one threshold of 50 %, meaning if the number of signals surpasses half of the total channels, the prediction is considered validated as SPC. The second threshold is set at 33 %, indicating that if more than one-third of the channels exhibit SPC, there is a higher possibility of SPC present on the track. When the number of channels indicating SPC falls below the

**Fig. 11.** SPC prediction shown with the SAWP per 10 m.

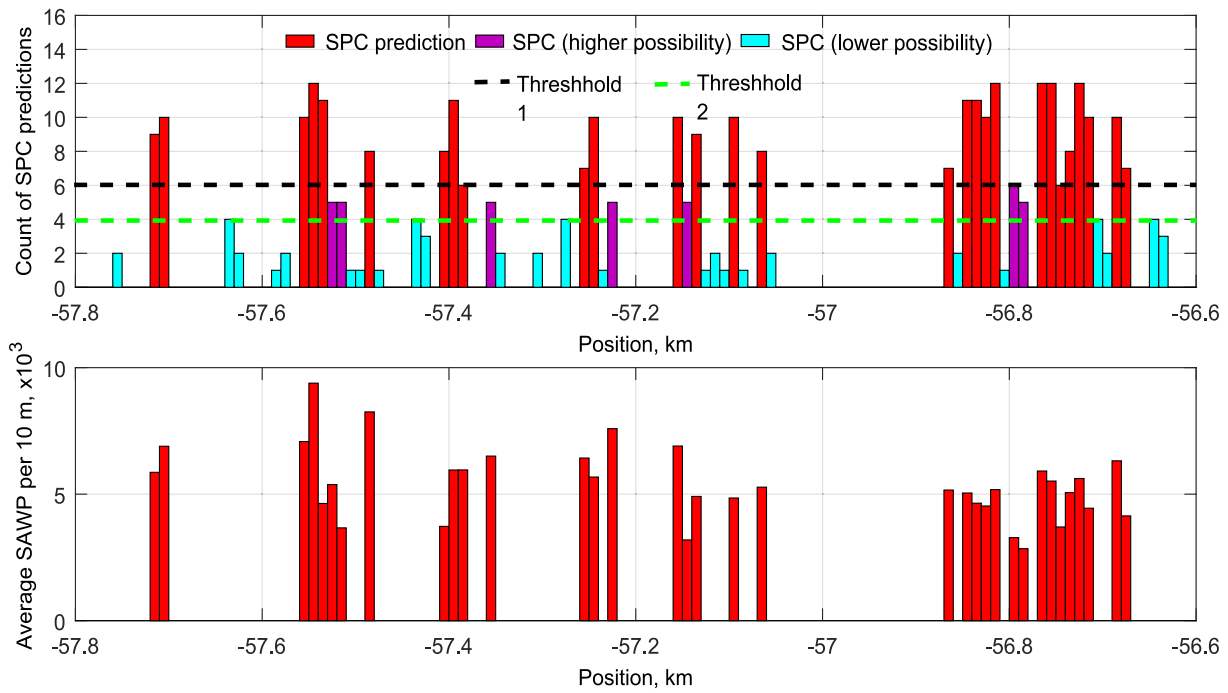


Fig. 12. Prediction of SPC, the possibility and severity in terms of SAWP per 10 m.

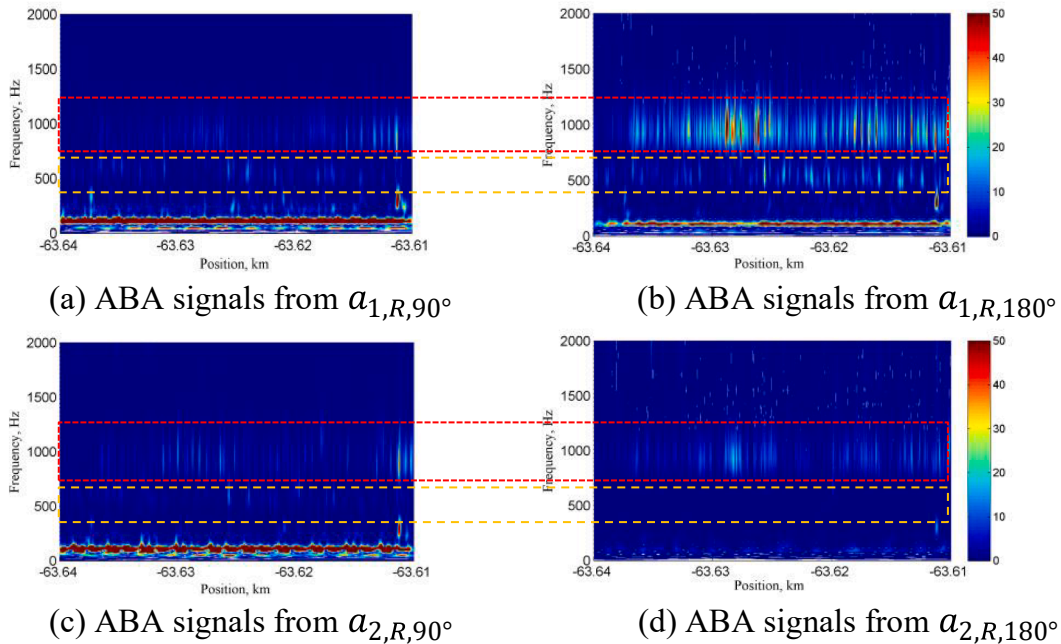


Fig. 13. Scalogram of ABA signals for accelerometer sensitivity analysis to the SPC ($v = 102.6$ km/h).

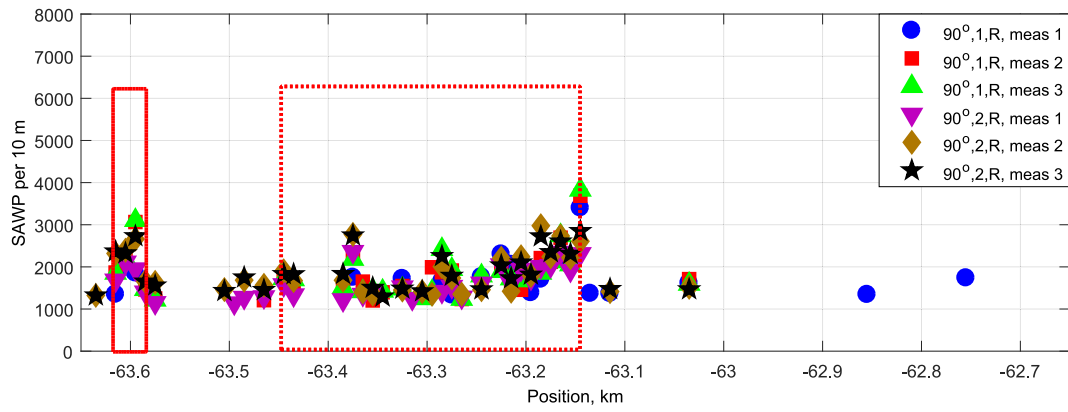
second threshold, the possibility of SPC becomes lower. The severity of SPC is evaluated based on the SAWP per 10 m. It is worth noting that when the prediction falls below the second threshold, indicating a low possibility of SPC, the corresponding SAWP per 10 m is not visible in the figure.

5.2. Case Study 2

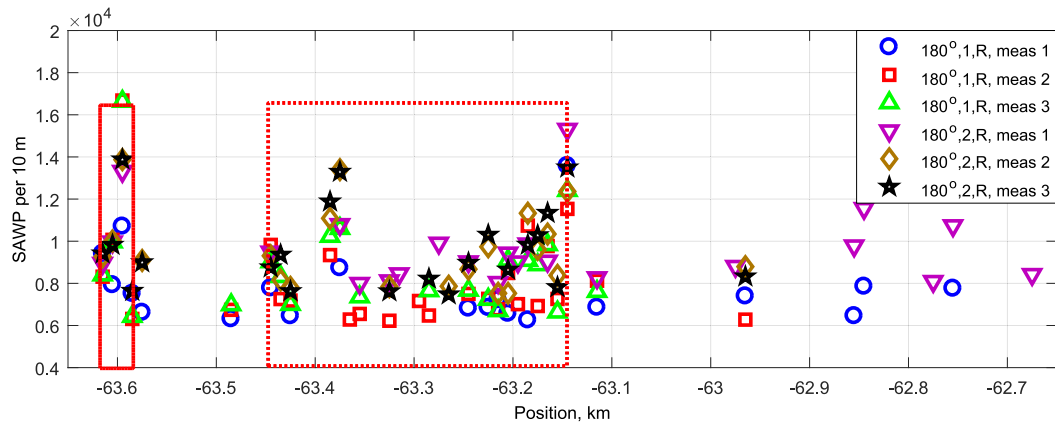
To provide additional validation for the proposed algorithm and

parameters, the analysis of the ABA signals from a different location is shown in Fig. 13. The ABA signals are from the right rail where the SPC is observed. Similar to the previous location, there is a notable energy concentration primarily within the frequency range of 700 Hz to 1600 Hz. Again, the same frequency component can be used for SPC detection. From the comparison of the SPC signals between detections and numerical simulations, it is confirmed that the time–frequency responses from the numerical simulations are valid.

Similarly, the SPC predictions for Case Study 2 are shown in Figs. 14



(a) Vertical ABA



(b) Longitudinal ABA

Fig. 14. SPC prediction shown with the SAWP per 10 m.

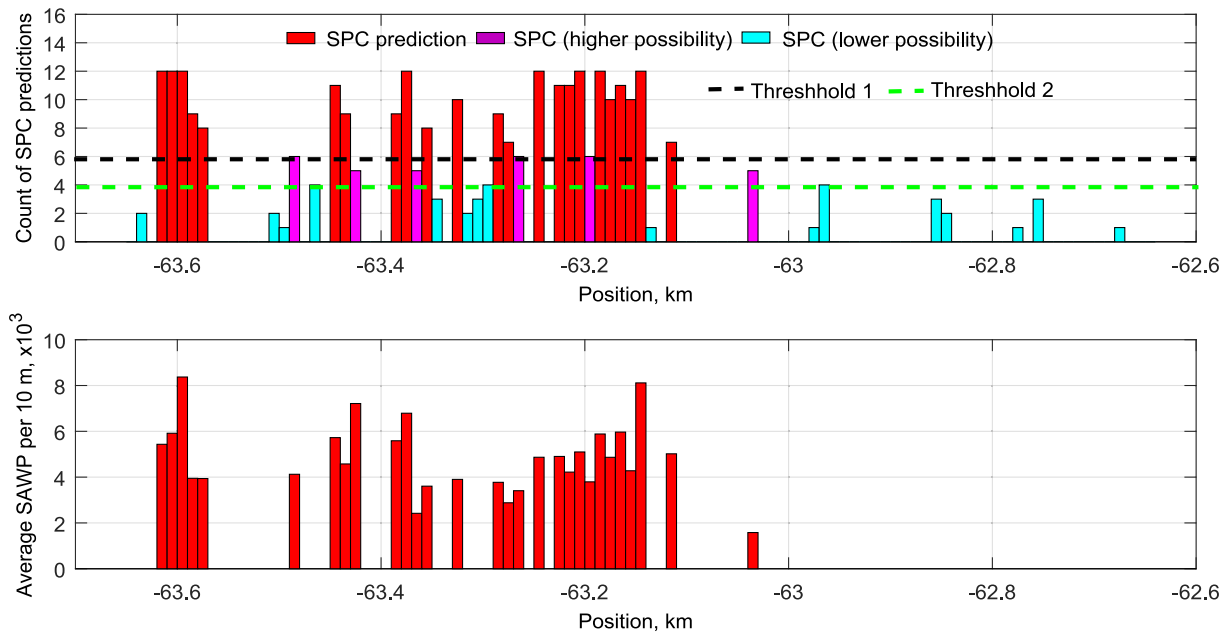


Fig. 15. Prediction of SPC, the possibility and severity in terms of SAWP per 10 m.

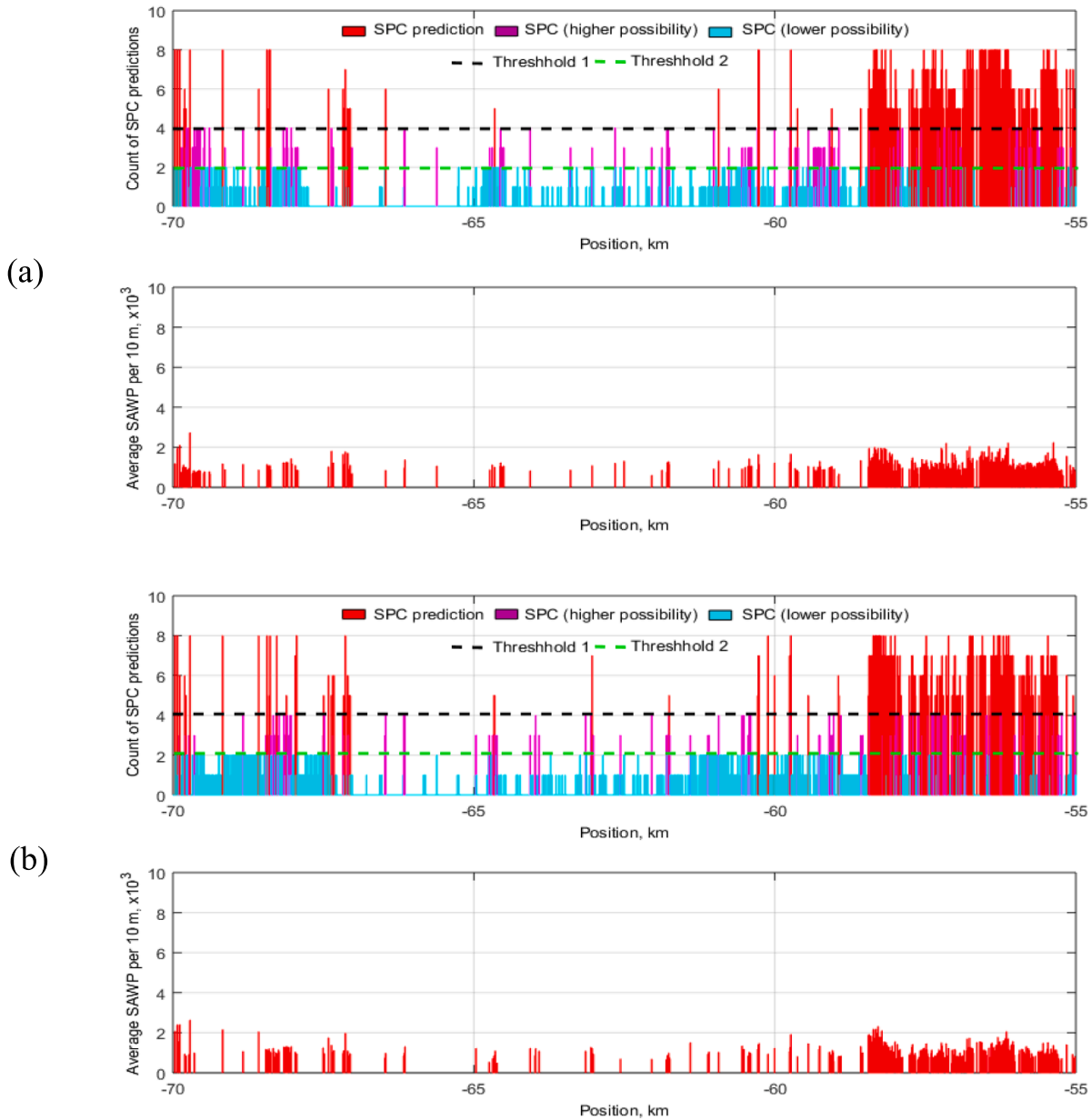


Fig. 16. Prediction of SPC, the possibility and severity in terms of SAWP per 10 m at (a) left rail, (b) right rail.

and 15. Shortly after the ABA measurement, a track visit is organized to record the SPC. The characteristics of the SPC in Case Study 2 are shown in Fig. 10b. The field recording of the SPC agrees well with the prediction. Hence, the developed algorithm is validated by detecting the SPC in this Case Study.

5.3. Global track prediction

With the validated algorithm for SPC detection, a prediction for the whole track between Assen and Groningen is made, as shown in Fig. 16. There are in total two measurement runs, in comparison to the previously considered 3 runs. Therefore, instead of 12, we will consider in total 8 signals used for the prediction. Two thresholds used for predicting the possibility of SPC are 50 % as before (4 counts), but 25 % in this case for the lower possibility (2 counts). The severity of the SPC is lower in comparison to the previous measurements analyzed in Sections

5.1 and 5.2. The reason is due to the grinding maintenance, which was performed nine months before the ABA measurement and removed the SPC. The prediction of the SPC is shown on the map with GPS in Fig. 17 to gain a general view. The detection of SPC as a low possibility, high possibility, and SPC are shown with different colors laying above the general track alignment. The rail surface in Case Study 1 is shown in Fig. 18. SPC still exists at this location but with lower severity.

5.4. Comparison before and after grinding

The above two case studies in Sections 5.1 and 5.2 are before grinding, and the results after grinding are compared in this section with their severities shown in Figs. 19 and 20, respectively. Due to the current detection algorithm using a relative SAWP value calculated from an average of the whole section of measurement, when the global rail roughness level is low, the detection algorithm gives a high resolution to

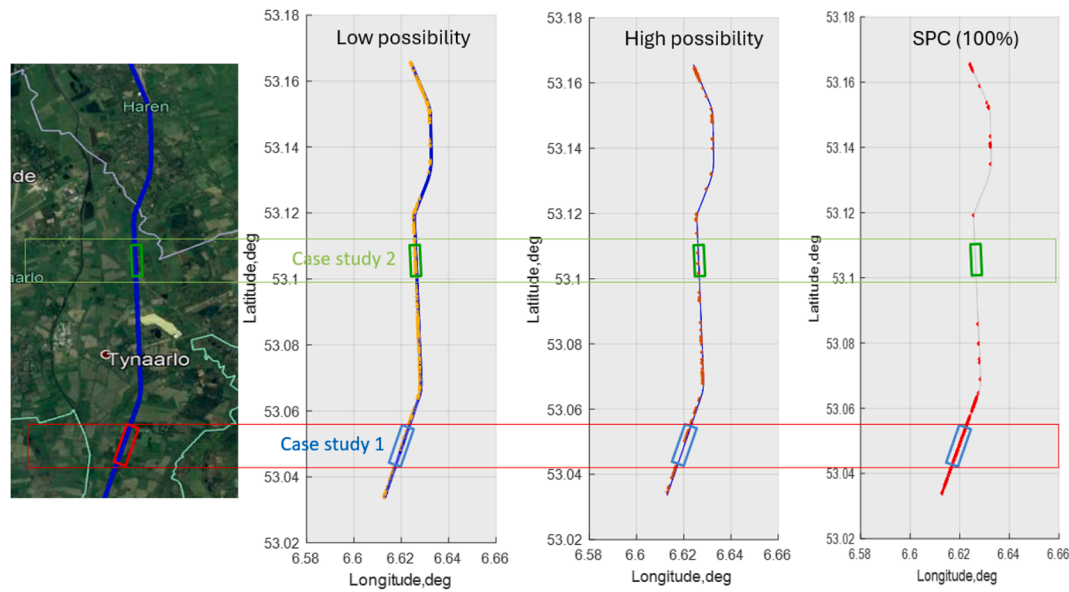


Fig. 17. Prediction of SPC shown in the map (Red dots indicate confirmed SPC, orange dots indicate a high possibility of SPC, and yellow dots indicate a low possibility of SPC). (For interpretation of the references to colour in this figure legend, the reader is referred to the web version of this article.)



Fig. 18. Rail with quite light SPC.

detect very light SPC. In this way, it can be shown that ABA can be used to evaluate the grinding quality. Before grinding, both locations in the figures below show SPC. However, after grinding, the section of track from Case Study 1 shows comparably higher vibration energy in the defined frequency range for SPC than the section of track from Case Study 2. This indicates that the rail surface roughness level in Case Study 2 should be smaller than that in Case Study 1.

6. Conclusions

This research focuses on utilizing ABA measurements to detect and monitor SPC in railway tracks. A 3D FE dynamic vehicle-track model is employed to identify the frequency responses of ABA signals corresponding to SPC. These responses are further validated using field ABA signals. The ABA signals with SPC are analyzed to facilitate the differentiation from other defects, particularly rail squats, which exhibit overlapping frequency ranges used for detection. Then, a detection algorithm for SPC is developed based on wavelet transform. The algorithm is validated with case studies and used to predict the SPC of the whole track. The key findings and summaries of this work are as follows:

- 1) The frequency response associated with SPC is successfully identified and validated by comparing the results from the 3D FE vehicle-track model with measured ABA signals at SPC locations.
- 2) Signals from different accelerometers instrumented at different directions in the axle box exhibit varying sensitivities to SPC. In the present case studies, longitudinal ABA exhibited higher sensitivity to SPC than vertical ABA within the investigated frequency range of 700–1600 Hz.
- 3) A detection algorithm is proposed based on the identified time–frequency responses at SPC. This algorithm serves as an indicator of both the possibility and severity of SPC.
- 4) The effectiveness of the algorithm is validated with two case studies, and its application is extended to predict SPC throughout the entire track between Assen and Groningen.

In addition, a whole track SPC prediction can be employed for the evaluation of maintenance operations. Further research should focus on validating numerical predictions by comparing them with ABA measurements at SPC locations obtained at different measurement speeds. Additionally, experimental methods to tune the parameters proposed in this paper will need to be developed, as additional field work is needed

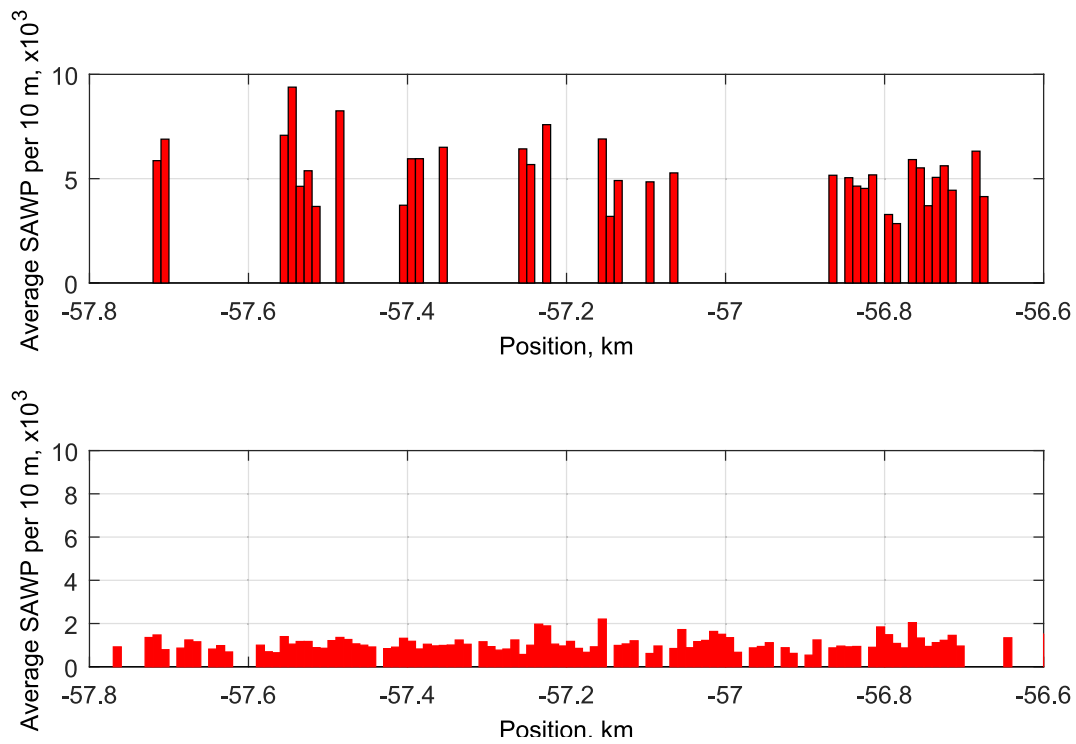


Fig. 19. Comparison of SPC severity before and after grinding: Case Study 1.

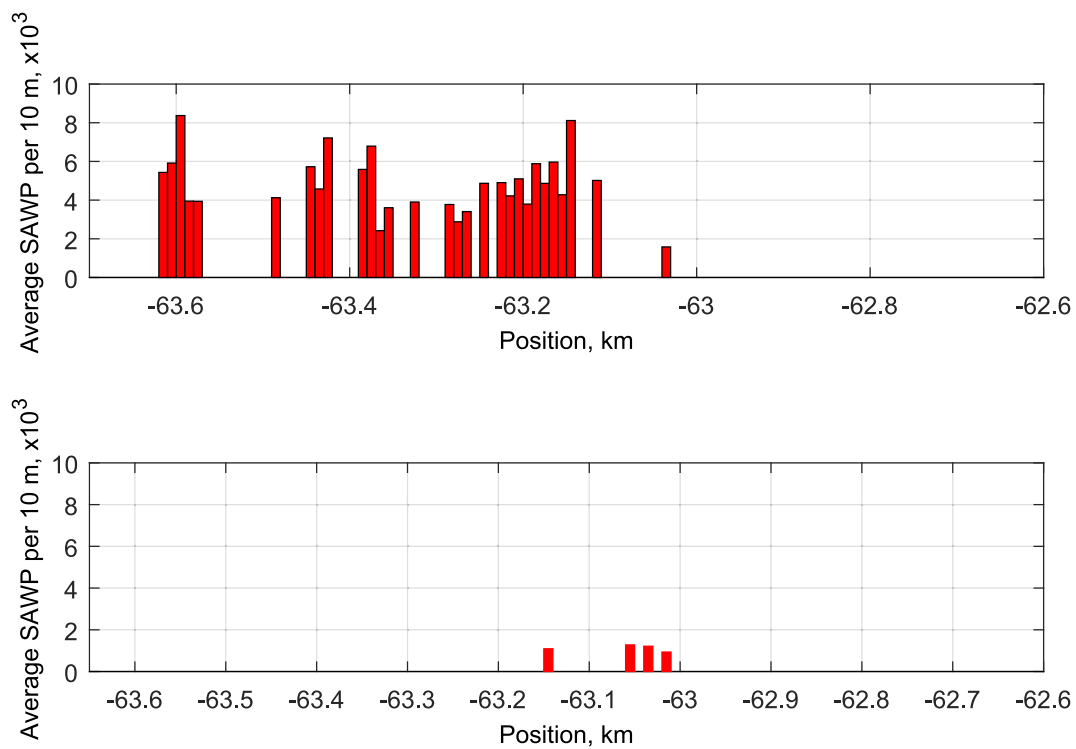


Fig. 20. Comparison of SPC severity before and after grinding: Case Study 2.

to establish the quantitative relations between ABA measurement and SPC characteristics such as amplitude or wavelength. Besides, the proposed method may not be directly applicable to tightly curved tracks or stations with strong speed variation, and this limitation should be addressed in future research.

CRediT authorship contribution statement

Shaoguang Li: Conceptualization, Data curation, Formal analysis, Investigation, Methodology, Validation, Visualization, Writing – original draft. **Pan Zhang:** Writing – review & editing, Visualization, Methodology, Investigation, Formal analysis. **Alfredo Núñez:** Writing –

review & editing, Visualization, Methodology, Investigation, Formal analysis. **Rolf Dollevoet**: Resources, Project administration, Funding acquisition, Conceptualization. **Zili Li**: Writing – review & editing, Supervision, Resources, Project administration, Methodology, Investigation, Funding acquisition, Conceptualization.

Declaration of competing interest

The authors declare that they have no known competing financial interests or personal relationships that could have appeared to influence the work reported in this paper.

Acknowledgments

This research is partly supported by ProRail.

Data availability

Data will be made available on request.

References

- [1] S. Grassie, J. Kalousek, Rail corrugation: characteristics, causes and treatments, *Proceedings of the Institution of Mechanical Engineers, Part f: Journal of Rail and Rapid Transit* 207 (1993) 57–68.
- [2] L. Ling, W. Li, H. Shang, X. Xiao, Z. Wen, X. Jin, Experimental and numerical investigation of the effect of rail corrugation on the behaviour of rail fastenings, *Veh. Syst. Dyn.* 52 (2014) 1211–1231.
- [3] X. Deng, Z. Qian, Z. Li, R. Dollevoet, Investigation of the formation of corrugation-induced rail squats based on extensive field monitoring, *Int. J. Fatigue* 112 (2018) 94–105.
- [4] X.-S. Jin, Key problems faced in high-speed train operation, *China's high-speed rail technology: an international, Perspective* (2018) 27–45.
- [5] Z. Li, S. Li, P. Zhang, A. Núñez, R. Dollevoet, Mechanism of short pitch rail corrugation: initial excitation and frequency selection for consistent initiation and growth, *International Journal of Rail Transportation* 12 (2024) 1–36.
- [6] P. Zhang, S. Li, Z. Li, Short pitch corrugation mitigation by rail constraint design, *Int. J. Mech. Sci.* 243 (2023) 108037.
- [7] J. Han, X. Xiao, Y. Wu, Z. Wen, G. Zhao, Effect of rail corrugation on metro interior noise and its control, *Appl. Acoust.* 130 (2018) 63–70.
- [8] S. Grassie, A practical methodology to prioritise reprofiling sites for corrugation removal, *Proceedings of the Institution of Mechanical Engineers, Part f: Journal of Rail and Rapid Transit* 234 (2020) 362–369.
- [9] H. Tanaka, M. Miwa, Modeling the development of rail corrugation to schedule a more economical rail grinding, *Proceedings of the Institution of Mechanical Engineers, Part f: Journal of Rail and Rapid Transit* 234 (2020) 370–380.
- [10] S.L. Grassie, Measurement of railhead longitudinal profiles: a comparison of different techniques, *Wear* 191 (1996) 245–251.
- [11] M. Ph Papaelias, C. Roberts, C.L. Davis, A review on non-destructive evaluation of rails: state-of-the-art and future development, *Proceedings of the Institution of Mechanical Engineers, Part F: Journal of Rail and rapid transit*, 222 (2008) 367–384.
- [12] Q. Li, S. Ren, A real-time visual inspection system for discrete surface defects of rail heads, *IEEE Trans. Instrum. Meas.* 61 (2012) 2189–2199.
- [13] RAILPROF, <https://www.esveld.com/railprof.html>.
- [14] S.L. Grassie, Rail corrugation: advances in measurement, understanding and treatment, *Wear* 258 (2005) 1224–1234.
- [15] A. Caprioli, A. Cigada, D. Raveglia, Rail inspection in track maintenance: a benchmark between the wavelet approach and the more conventional fourier analysis, *Mech. Syst. Sig. Process.* 21 (2007) 631–652.
- [16] Z. Wei, X. Sun, F. Yang, Z. Ke, T. Lu, P. Zhang, C. Shen, Carriage interior noise-based inspection for rail corrugation on high-speed railway track, *Appl. Acoust.* 196 (2022) 108881.
- [17] L. Chen, Y. Li, X. Zhong, Q. Zheng, H. Liu, An automated system for position monitoring and correction of chord-based rail corrugation measuring points, *IEEE Trans. Instrum. Meas.* 68 (2018) 250–260.
- [18] P. Wang, Y. Wang, H. Tang, M. Gao, R. Chen, J. Xu, Error theory of chord-based measurement system regarding track geometry and improvement by high frequency sampling, *Measurement* 115 (2018) 204–216.
- [19] L. Niu, F. Yang, X. Deng, P. Zhang, G. Jing, W. Qiang, Y. Guo, An assessment method of rail corrugation based on wheel–rail vertical force and its application for rail grinding, *J. Civ. Struct. Heal. Monit.* 13 (2023) 1131–1150.
- [20] E. Resendiz, J.M. Hart, N. Ahuja, Automated visual inspection of railroad tracks, *IEEE Trans. Intell. Transp. Syst.* 14 (2013) 751–760.
- [21] M. Nieniewski, Morphological detection and extraction of rail surface defects, *IEEE Trans. Instrum. Meas.* 69 (2020) 6870–6879.
- [22] Q. Xie, G. Tao, S.M. Lo, X. Yang, Z. Wen, A data-driven convolutional regression scheme for on-board and quantitative detection of rail corrugation roughness, *Wear* 524 (2023) 204770.
- [23] S. Unsiwilai, L. Wang, A. Núñez, Z. Li, Multiple-axle box acceleration measurements at railway transition zones, *Measurement* 213 (2023) 112688.
- [24] S. Unsiwilai, W. Phusakulkajorn, C. Shen, A. Zoeteman, R. Dollevoet, A. Núñez, Z. Li, Enhanced vertical railway track quality index with dynamic responses from moving trains, *Heliyon* 10 (2024).
- [25] Z. Li, M. Molodova, A. Núñez, R. Dollevoet, Improvements in axle box acceleration measurements for the detection of light squats in railway infrastructure, *IEEE Trans. Ind. Electron.* 62 (2015) 4385–4397.
- [26] B. An, P. Wang, J. Xu, R. Chen, D. Cui, Observation and simulation of axle box acceleration in the presence of rail weld in high-speed railway, *Appl. Sci.* 7 (2017) 1259.
- [27] Y. Zhou, J. Vuitton, Q. Tian, M. Hecht, Wheel flat detection by using the angular domain synchronous averaging method and axle box acceleration: simulation and experiment, *Measurement* 230 (2024) 114508.
- [28] J. Nielsen, E. Berggren, T. Lölgen, R. Müller, Overview of methods for measurement of track irregularities, *RIVAS Railway Induced Vibration Abatement Solutions Collaborative Project* (2013).
- [29] S.L. Grassie, in: *Measurement of Longitudinal Irregularities on Rails Using an Axlebox Accelerometer System*, in: *Noise and Vibration Mitigation for Rail Transportation Systems*, Ghent, Belgium, Springer, 2021, pp. 320–328.
- [30] L. Faccini, J. Karaki, E. Di Gialleonardo, C. Somaschini, M. Bocciolone, A. Collina, A methodology for continuous monitoring of rail corrugation on Subway lines based on axlebox acceleration measurements, *Appl. Sci.* 13 (2023) 3773.
- [31] S. Li, A. Núñez, Z. Li, R. Dollevoet, Automatic detection of corrugation: Preliminary results in the Dutch network using axle box acceleration measurements, in: *ASME/IEEE Joint Rail Conference, American Society of Mechanical Engineers*, 2015, pp. V001T001A023.
- [32] M. Molodova, M. Oregui, A. Núñez, Z. Li, R. Dollevoet, Health condition monitoring of insulated joints based on axle box acceleration measurements, *Eng. Struct.* 123 (2016) 225–235.
- [33] C. Torrence, G.P. Compo, A practical guide to wavelet analysis, *Bull. Am. Meteorol. Soc.* 79 (1998) 61–78.
- [34] S. Li, Z. Li, A. Núñez, R. Dollevoet, New insights into the short pitch corrugation enigma based on 3D-FE coupled dynamic vehicle-track modeling of frictional rolling contact, *Appl. Sci.* 7 (2017) 807.
- [35] M. Molodova, Z. Li, R. Dollevoet, Axle box acceleration: measurement and simulation for detection of short track defects, *Wear* 271 (2011) 349–356.
- [36] R. Courant, K. Friedrichs, H. Lewy, On the partial difference equations of mathematical physics, *IBM J. Res. Dev.* 11 (1967) 215–234.
- [37] M. Molodova, Z. Li, A. Núñez, R. Dollevoet, Automatic detection of squats in railway infrastructure, *IEEE Trans. Intell. Transp. Syst.* 15 (2014) 1980–1990.